







Cite this: *Chem. Sci.*, 2024, 15, 1061

All publication charges for this article have been paid for by the Royal Society of Chemistry

Enhancing the photocatalytic upcycling of polystyrene to benzoic acid: a combined computational-experimental approach for acridinium catalyst design†

Albert Ong, ^{‡a} Zi Cheng Wong, ^{‡b} Kang Le Osmund Chin, ^c Wei Wei Loh, ^a Ming Hui Chua, ^{*c} Shi Jun Ang ^{*bc} and Jason Y. C. Lim ^{*ad}

Converting polystyrene into value-added oxygenated aromatic compounds is an attractive end-of-life upcycling strategy. However, identification of appropriate catalysts often involves laborious and time-consuming empirical screening. Herein, after demonstrating the feasibility of using acridinium salts for upcycling polystyrene into benzoic acid by photoredox catalysis for the first time, we applied low-cost descriptor-based combinatorial *in silico* screening to predict the photocatalytic performance of a family of potential candidates. Through this approach, we identified a non-intuitive fluorinated acridinium catalyst that outperforms other candidates for converting polystyrene to benzoic acid in useful yields at low catalyst loadings (≤ 5 mol%). In addition, this catalyst also proved effective with real-life polystyrene waste containing dyes and additives. Our study underscores the potential of computer-aided catalyst design for valorizing polymeric waste into essential chemical feedstock for a more sustainable future.

Received 29th November 2023

Accepted 7th December 2023

DOI: 10.1039/d3sc06388g

rsc.li/chemical-science

1. Introduction

Polystyrene (PS), one of the most produced thermoplastics worldwide,¹ is indispensable in the packaging and construction industries.² However, it has become one of the most prevalent pollutants in the environment³ due to its chemical inertness and resulting slow rates of natural degradation. Because of the low existing global collection and recycling rates,⁴ the existing life-cycle of PS is largely linear, with expanded PS constituting a large fraction of landfill waste.⁵ Instead of disposal, upcycling end-of-life plastics into financially more-valuable chemicals and materials is of great interest,^{6–10} with PS being especially valued as a possible source of industrially-relevant aromatics.^{11,12} Amongst them, benzoic acid (BA) is of particular importance, with annual demand exceeding 500 000 metric tons¹³ across

multiple industrial applications, such as food preservatives, antimicrobial agents and chemical precursors. However, PS oxidative degradation is hindered by the chemical inertness of its saturated C–C backbone, which traditionally necessitates harsh oxidation conditions involving high temperatures and pressures.^{14–16}

Photoredox catalysis offers unique opportunities for PS degradation to occur under mild conditions (*e.g.* near-ambient temperature) to produce oxygenated aromatics.^{17–20} This stems from their ability to facilitate hydrogen atom transfer (HAT) from the PS backbone, generating reactive radicals that elicit backbone oxidation and chain scission reactions. Although several inorganic catalysts have been reported to produce oxygenated aromatics from PS,^{18,21} the use of metal-free low molecular weight organo-photoredox catalysts²² has thus far been largely under-exploited. In this respect, we hypothesized that acridinium salts, which are able to access highly-oxidizing excited states upon visible light photo-activation,²³ can serve as effective catalysts for PS oxidative degradation. Furthermore, low-energy visible light photoexcitation of acridinium salts can also enable better control of PS backbone degradation to achieve improved product selectivity. Acridinium salts are amongst the most structurally-diverse families of organo-photoredox catalysts available, offering ample opportunities to modulate their photophysical properties (*e.g.* excited state redox potential) and catalytic efficacy by diversification of the scaffold substituents.²⁴ However, this makes a systematic empirical exploration of the vast catalyst design space for PS degradation impractically

^aInstitute of Materials Research and Engineering (IMRE), Agency for Science, Technology and Research (A*STAR), 2 Fusionopolis Way, Innova #08-03, Singapore 138634, Republic of Singapore. E-mail: jason_lim@imre.a-star.edu.sg

^bInstitute of High Performance Computing (IHPC), Agency for Science, Technology and Research (A*STAR), 1 Fusionopolis Way, Connexis, #16-16, Singapore 138632, Republic of Singapore. E-mail: ang_shi_jun@ihpc.a-star.edu.sg

^cInstitute of Sustainability for Chemicals, Energy and Environment (ISCE2), Agency for Science, Technology and Research (A*STAR), 1 Pesek Road, Jurong Island, Singapore 627833, Republic of Singapore. E-mail: chua_ming_hui@isce2.a-star.edu.sg

^dDepartment of Materials Science and Engineering, National University of Singapore (NUS), 9 Engineering Drive 1, Singapore 117576, Republic of Singapore

† Electronic supplementary information (ESI) available. See DOI: <https://doi.org/10.1039/d3sc06388g>

‡ These authors contributed equally to the manuscript.

laborious, with multi-stepped *de novo* synthesis of each acridinium candidate required. To overcome this bottleneck, we present a combined experimental and computational catalyst screening approach,²⁵ allowing us to identify a high-performing fluorinated acridinium catalyst candidate able to produce BA with yield surpassing other structural analogues synthesized.

2. Results and discussion

As PS degradation using acridinium salts is hitherto unexplored, we commenced the study with the model **Ph-Acr-Ph** catalyst (nomenclature: [9-substituent]-Acr-[N-substituent]) to identify the essential reaction conditions for BA production from commercial PS resins (Table 1). When irradiated with a 390 nm LED light source for 24 h under an O₂ atmosphere (entry 1), **Ph-Acr-Ph** (10 mol% w.r.t. PS monomers) and 10 mol% HCl (aq) afforded BA in 33% yield as the dominant aromatic product, with some formic acid detected (Fig. S4†). Trace aromatic molecules such as benzaldehyde were also detected by ESI-MS (Fig. S5 and S23†), but were present in insufficient quantities for ¹H NMR detection. In addition, gel permeation chromatography (GPC) analysis of the crude product mixture revealed that short-chain oligomers with a bimodal distribution (Fig. S6†) were also formed during the reaction.

Several reactions were then performed to understand the conditions necessary for BA production to occur from PS. Control experiments (entries 2–4) confirmed that **Ph-Acr-Ph**, O₂ and light were essential for efficient BA generation, and replacing the O₂ atmosphere with air (21% O₂) resulted in greatly reduced reaction efficacy (Table S1†). It is noteworthy that although the reaction under argon (Table 1, entry 3) did not yield any BA, PS

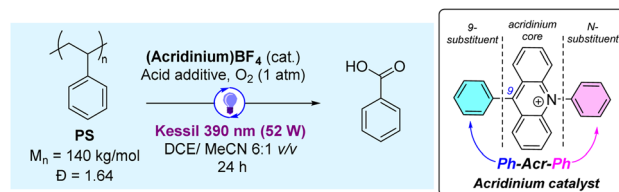
chain cleavage occurred (Fig. S10†), possibly brought about by C–C radical chain cleavage initiated by hydrogen abstraction from the PS backbone by the photoexcited acridinium catalyst (*vide infra*). This hypothesis is supported by the lack of PS chain cleavage in the dark (entry 4, Fig. S12†), which prevented acridinium excited state formation. A substantial reduction in BA yield resulted without HCl (Table 1, entry 5) and when HCl was replaced with an equivalent quantity of water (Table S1†), indicating the synergistic involvement of Cl[−] and **Ph-Acr-Ph** in PS degradation, plausibly through generation of chlorine radicals (*vide infra*).²⁶ Increasing the HCl loading to 200 mol% afforded higher BA yields despite lowering the **Ph-Acr-Ph** loading to 5 mol% (entry 6), though larger quantities of HCl (500 mol%) only led to marginally more BA production (entry 7). Notably, 200 mol% HCl alone without **Ph-Acr-Ph** only afforded BA with 6% yield (Table S1†), underscoring the catalyst's importance even in the presence of large excess of HCl. When HCl was replaced with HBr in the presence of **Ph-Acr-Ph**, much poorer BA yields resulted (entry 8). While Br[−] is easier to oxidize than Cl[−] to generate their respective radicals ($E_{\text{Br}^{\cdot}/\text{Br}^-}^{\circ} = 1.60 \text{ V vs. SCE}$, $E_{\text{Cl}^{\cdot}/\text{Cl}^-}^{\circ} = 2.03 \text{ V vs. SCE}$),²⁷ HAT from PS by Cl[•] is favoured due to the stronger H–Cl bond formed (bond dissociation energy for H–Cl = 103 kcal mol^{−1}; H–Br = 87 kcal mol^{−1}).^{28,29} The best BA yields were obtained using DCE/MeCN 6 : 1 (v/v), with MeCN, CHCl₃ and different DCE-containing solvent mixtures affording much less BA (Table S1†). Finally, the reaction is tolerant to different excitation wavelengths, with 440 nm irradiation affording similar BA yields (entry 9) as 390 nm.

Fig. 1A outlines a possible mechanism for photoredox oxidative PS conversion to BA, based on our empirical observations and by analogy to reported mechanisms of acridinium-

Table 1 Reaction screening for acridinium-catalysed PS photoredox degradation^a

S/N	Ph-Acr-Ph loading ^a (mol%)	Acid additive ^b (mol% loading)	Deviation from above conditions	BA yield ^c (%)	M_n^d (kDa)
1	10	HCl (10)	—	33	<0.30 ^{e,f}
2	—	HCl (10)	—	6	1.71
3	10	HCl (10)	Argon atmosphere	0	6.90
4	10	HCl (10)	Reaction in the dark	0	42.3
5	10	—	—	20	<0.30 ^{e,f}
6	5	HCl (200)	—	46	<0.30 ^{e,f}
7	5	HCl (500)	—	50	<0.30 ^{e,f}
8	5	HBr (200)	—	7	5.56 ^f
9	5	HCl (200)	440 nm irradiation	43	<0.30 ^f

^a Although no external heat source was used, the reaction temperature was maintained at ($\sim 35 \pm 1$) °C throughout reaction duration due to heating caused by the LED light source. ^b w.r.t. PS monomers present. ^c Determined by quantitative ¹H-NMR using 1,3,5-trimethoxybenzene as internal standard (Section S4). ^d Determined *via* GPC analysis with THF as the mobile phase against monodisperse polystyrene standards. ^e M_n of PS starting material = 42.7 kDa by GPC analysis. ^f Molecular weight of PS oligomers are lower than the accurate GPC mass range. ^g Bimodal GPC product distribution observed.



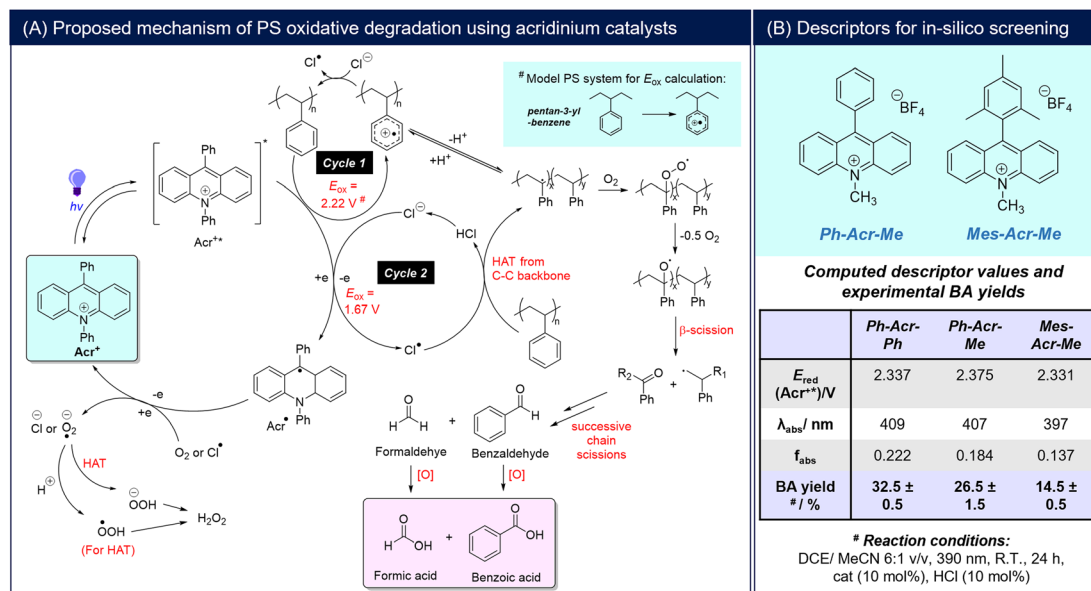


Fig. 1 (A) Proposed mechanism for photoredox catalysed oxidative degradation with acridinium salts; (B) computed photophysical (λ_{abs} and f_{abs}) and excited state redox ($E_{\text{red}}(\text{Acr}^{+*})$) properties of three model acridinium salts, with their empirical BA yields. Computed E_{ox} and E_{red} values are w.r.t. SHE. # Yields are calculated from an average of two repeat experiments.

mediated arene oxidations.^{22,23} Photoexcitation of the catalyst generates its excited state (Acr^{+*}), which promotes a one-electron oxidation of PS to form a reactive PS^{+*} intermediate that can undergo deprotonation to generate a benzylic radical (Cycle 1).^{30,31} The generated PS^{+*} may also oxidise Cl^- to Cl^{\bullet} (calculated E_{ox} of model PS compound, pentan-3-yl-benzene, $> E_{\text{ox}}(\text{Cl}^-)$) (Section S5†). In addition, the Cl^{\bullet} generated from Acr^{+*26} can promote HAT from the PS backbone (Cycle 2).¹⁸ The common benzylic radical formed from both catalytic cycles can be trapped by O_2 to form a peroxo intermediate that can further undergo homolytic O–O cleavage to form an oxo-radical species. β -Scission then forms a primary radical chain end and a phenyl ketone that can further react, propagating chain cleavage to ultimately give BA and formic acid as the terminal oxidized products. Although a $[\text{PS}\cdots\text{H}^+]$ adduct from interactions of PS with acids has been proposed to facilitate PS degradation by acting as a photosensitiser for $^1\text{O}_2$ generation,¹⁹ this is unlikely to play a significant role under our present reaction conditions, as the presence of HCl and HBr alone without acridinium catalysts afforded only poor BA yields at 390 nm irradiation (Tables 1, S1†).

Due to the mechanistic complexity of photoredox oxidative PS degradation, a full mechanism-based *in silico* approach for catalyst screening is extremely demanding computationally.^{32–34} Thus, as a reasonable compromise for computational workload and accuracy, a descriptor-based approach was adopted.^{35,36} To perform the catalyst screening logically, photophysical and thermodynamic parameters satisfying essential mechanistic criteria from Fig. 1A were chosen.³⁷ Firstly, the ability of Acr^{+*} to initiate Cycles 1 and 2 must be thermodynamically feasible, *i.e.* $E_{\text{red}}(\text{Acr}^{+*}) > E_{\text{ox}}(\text{PS})$ and $E_{\text{ox}}(\text{Cl}^-)$. Secondly, the acridinium salt should possess appropriate photophysical properties allowing

access to a high concentration of Acr^{+*} during the reaction. In this regard, the catalyst should have λ_{abs} close to the irradiation wavelength (390 nm) and possess high oscillator strength (f_{abs}). Experimentally, the oscillator strength for an electronic transition can be calculated using the area under its corresponding absorption band.³⁸ As the height of the absorption band is simply the molar absorptivity at a given wavelength, the oscillator strength calculated using TD-DFT can be used to obtain the molar absorptivity. In the context of the present study, a higher value for the oscillator strength (or molar absorptivity) would thus imply a larger concentration of acridinium salt being electronically excited upon photostimulation, which should in turn lead to an improvement in the overall BA yield. In order to evaluate the descriptors that could serve as a reasonable predictors of catalyst performance, we computed the $E_{\text{red}}(\text{Acr}^{+*})$, λ_{abs} and f_{abs} values of three model acridinium salts (**Ph-Acr-Ph**, **Ph-Acr-Me** and **Mes-Acr-Me**) (details of TD-DFT calculations in Section S5†), and evaluated them against the yields of BA obtained from PS under identical reaction conditions (Fig. 1B). Notably, we verified that TD-DFT calculations were able to provide reasonable estimates of the actual experimental values of $E_{\text{red}}(\text{Acr}^{+*})$ and λ_{abs} (Tables S2 and S4† with associated discussions). In all cases, BA was produced, albeit with different yields. This supported the thermodynamic feasibility of both catalytic cycles with calculated $E_{\text{red}}(\text{Acr}^{+*})$ for all catalysts $> E_{\text{ox}}(\text{PS})$ and $E_{\text{ox}}(\text{Cl}^-)$. Amongst the descriptors, f_{abs} emerged as the best predictor of catalyst performance, with higher values correlating to better BA yields.

Combinatorial catalyst screening was then performed *in silico* on a family of acridinium salts bearing different 9-/N-substituents to identify candidates that can possibly outperform **Ph-Acr-Ph** for PS degradation (Fig. 2A). Despite only



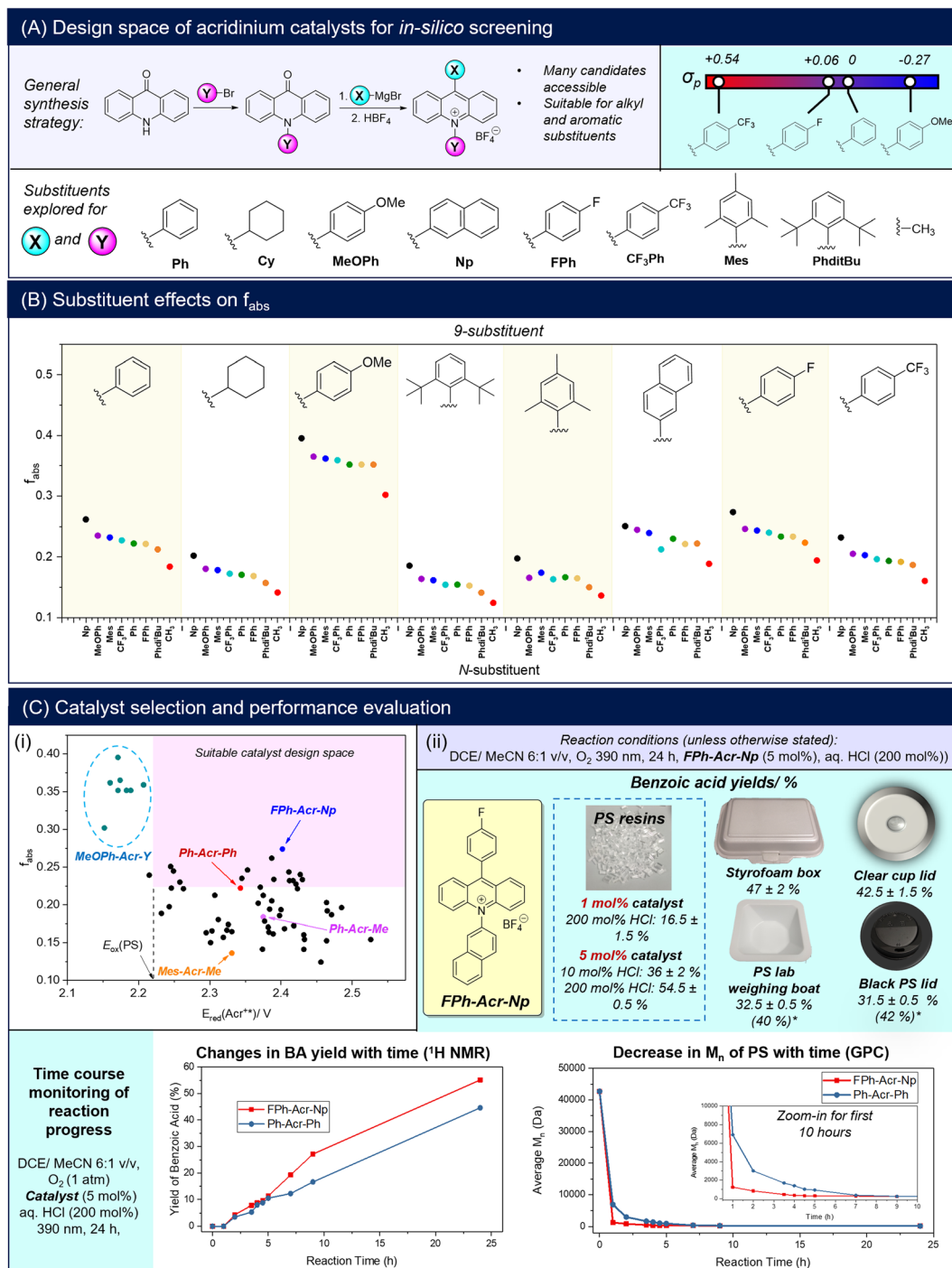


Fig. 2 Acridinium catalyst prediction and experimental validation: (A) general synthetic scheme of acridinium salts, the substituent chemical space for *in silico* screening and selected Hammett substituent constants (σ_p);³⁹ (B) scatter plot of acridinium f_{abs} with different substituents at the 9- and N-positions; (C)(i) scatter plot of $E_{\text{red}}(\text{Acr}^{+*})$ and f_{abs} of the screened chemical space, with the region in pink enclosing candidates predicted to have better PS degradation performance than the Ph-Acr-Ph baseline; (ii) BA yields from PS resins and real-life waste using the selected FPh-Acr-Np catalyst, and time course experiments showing the evolution of BA yields and PS molecular weight with increasing reaction duration. Yields are calculated from an average of two repeat experiments (*yields in parentheses consider removal of insoluble additives such as dyes).

varying the 9-/N-substituents, the combinatorial catalyst design space is vast, with >1000 possible substituent candidates for each position from a Reaxys® substructure search. As a proof-of-concept, we selected a group of substituents representing

electron-rich and electron-deficient aromatics, alkyl and extended π -systems for *in silico* screening (Section S5†). Fig. 2B illustrates the effects of each 9-/N-substituent on the acridinium salt's f_{abs} values. Generally, 9-substituents exert a larger



influence on the f_{abs} compared to *N*-substituents, as they contribute to both the locally-excited and charge transfer excited states in the acridinium salts (see Section S5†). Amongst the *para*-functionalised aryl substituents at the 9-position, f_{abs} decreases as substituents become more electron-deficient ($\text{MeOPh} > \text{Ph} \approx \text{FPh} > \text{CF}_3\text{Ph}$), reflected by more positive Hammett substituent constants (Fig. 2A). Notably, this trend does not apply to the *N*-substituents, with the *N*-naphthyl unit affording the highest f_{abs} values for each 9-substituent series. In accordance with expectations however, more electron-withdrawing aryl units generally render the activated Acr^{+*} catalyst stronger oxidants, with calculated $E_{\text{red}}(\text{Acr}^{+*})$ values decreasing in the order $\text{CF}_3\text{Ph} > \text{FPh} > \text{Ph} > \text{MeOPh}$ regardless of their location on the *N*- or 9-positions (Table S5†).

Although f_{abs} was determined to be the primary predictor of BA yield, it is insufficient by itself for catalyst selection. The importance of the candidates also satisfying $E_{\text{red}}(\text{Acr}^{+*}) > E_{\text{ox}}(\text{PS})$ is evident from the **MeOPh-Acr-Y** family of catalysts. Although they possess the highest f_{abs} values amongst the candidates screened, their calculated $E_{\text{red}}(\text{Acr}^{+*})$ values were unfavorable (Fig. 2C(i)) (see Section S5† for a full discussion).^{40,41} Indeed, **MeOPh-Acr-Ph** was synthesized and experimentally verified to not produce any BA from PS degradation using 390 or 440 nm irradiation (Table S1†). With this established, an acridinium candidate with better PS degradation performance than the **Ph-Acr-Ph** benchmark can be identified in the chemical space bounded by $f_{\text{abs}}(\text{candidate}) > f_{\text{abs}}(\text{Ph-Acr-Ph})$ and $E_{\text{red}}(\text{Acr}^{+*}) > E_{\text{ox}}(\text{PS})$ (Fig. 2C(i)). The candidate possessing the highest f_{abs} value within this space, **FPh-Acr-Np**, was identified as the target catalyst (Fig. 2C(ii)) and synthesized (Section S2†). Gratifyingly, it could convert PS into BA with superior yields (of up to 55%) at 5 mol% catalyst loading compared to **Ph-Acr-Ph** at both low and high HCl loadings, further validating the effectiveness of our descriptor-based screening approach. It is noteworthy that when we lowered the **FPh-Acr-Np** loading to 1 mol% to evaluate the limits of catalyst loading, BA could still be obtained in 16.5% yield (Fig. 2C(ii)). Compared with existing reported homogeneous photoredox catalysts reported to degrade PS into oxygenated aromatics (Section S6†),^{18–21,42,43} the catalytic turnover of **FPh-Acr-Np** was amongst the best, and is especially advantaged by the low catalyst loadings required using our reaction conditions.

Time course experiments were then performed to elucidate the influences of **FPh-Acr-Np** on PS chain degradation and BA evolution compared with **Ph-Acr-Ph**. For both catalysts, tracking BA production by ^1H NMR analysis revealed that negligible quantities of BA were produced in the first hour (Fig. S50†), but thereafter increased continuously throughout the entire reaction duration (Fig. 2D(ii)). Despite this, a drastic drop in average M_n was observed in the first hour for both reactions catalysed by **FPh-Acr-Np** and **Ph-Acr-Ph**. This indicated that the first hour was dominated by propagating oxidative radical chain scission of the PS polymer backbones (Fig. 1A), before formation of benzoic acid, the terminal product of the oxidative degradation, could occur. Significantly, PS deconstruction catalysed by **FPh-Acr-Np** reduced the average M_n of the polymer at significantly

faster rate compared to that catalysed by **Ph-Acr-Ph**. From the 42.7 kDa PS resin, the M_n of the oxidized oligomers reached 1.26 kDa and 6.90 kDa within the first hour for **FPh-Acr-Np** and **Ph-Acr-Ph**, whilst requiring 5 and 9 h to reach the lower limit of GPC molecular weight detection, respectively. This further demonstrated the superiority of **FPh-Acr-Np** for PS degradation, further validating the effectiveness of our screening approach.

Finally, we demonstrated the generality of **FPh-Acr-Np** for PS oxidative upcycling using several real-life PS products (Fig. 2C(ii)). All products tested were well-tolerated, generating BA in synthetically-useful yields and demonstrating that **FPh-Acr-Np** was compatible with common additives such as plasticisers. It is noteworthy that although the dye in the black lid was shown to inhibit degradation,¹⁸ we overcame this problem using a solvent system that selectively dissolved the PS polymer but not the black dye, effectively upcycling the polymer into BA.

3. Conclusion

In conclusion, we have demonstrated for the first time that acridinium salts can be potent photoredox catalysts for oxidative degradation of PS to afford industrially-relevant BA at near-ambient temperature and pressure. Through the identification of key thermodynamic and photophysical descriptors, an *in silico* screening of acridinium analogues enabled the rapid identification of a high-performing **FPh-Acr-Np** catalyst candidate that could afford superior BA yields compared to all other benchmark acridinium catalysts attempted. The synergistic activity of **FPh-Acr-Np** and HCl for PS deconstruction allowed low catalyst loadings to be used (<5 mol%), and was also highly-compatible with real-life PS waste. Advantageously, the potential low toxicity of acridinium salts, evident from their many applications in bioimaging,^{44–46} may be beneficial if trace metal contamination is of concern for the BA's targeted application (especially in biomedical or food and beverage applications). Although only a sample of the acridinium chemical design space was sampled herein, our proof-of-concept study highlights the immense untapped potential of computer-aided catalyst design for low-energy and highly efficient upcycling of plastics and possibly, biomass (*e.g.* lignin), into essential chemicals.

Data availability

All experimental details and data supporting the findings of this study are available within the paper and its ESI.†

Author contributions

J. Y. C. L, S. J. A. and M. H. C. conceptualised the research. A. O. and K. L. O. C. performed synthesis and characterisation of all the catalyst. A. O. performed all the experimental screenings, data curation and validation. W. W. L. performed all GPC analyses of product mixtures. Z. C. W. and S. J. A. performed all the computational studies, data curation and validation. J. Y. C. L. wrote the manuscript with input from all authors.



Conflicts of interest

There are no conflicts to declare.

Acknowledgements

J. Y. C. Lim. is grateful to the NRF Fellowship (Award number: NRF-NRFF15-2023-0007) and the A*STAR Central Research Fund (UIBR) for generous funding support of this work. M. H. Chua acknowledges funding support by the A*STAR 2020 Career Development Fund (Grant Number: C210112042). This work was supported by the A*STAR Computational Resource Centre through the use of its high performance computing facilities. The authors acknowledge Dr Hazel Lau (A*STAR, IMRE) for assistance with ESI mass spectrometry analyses.

Notes and references

- 1 R. Geyer, J. R. Jambeck and K. L. Law, Production, use, and fate of all plastics ever made, *Sci. Adv.*, 2017, **3**(7), e1700782.
- 2 J. Maul, B. G. Frushour, J. R. Kontoff, H. Eichenauer, K.-H. Ott and C. Schade, Polystyrene and styrene copolymers, in *Ullmann's Encyclopedia of Industrial Chemistry*, 2007.
- 3 S. S. Yang, A. M. Brandon, D. F. Xing, J. Yang, J. W. Pang, C. S. Criddle, N. Q. Ren and W. M. Wu, Progresses in Polystyrene Biodegradation and Prospects for Solutions to Plastic Waste Pollution, *IOP Conf. Ser.: Earth Environ. Sci.*, 2018, **150**(1), 012005.
- 4 A. Rahimi and J. M. García, Chemical recycling of waste plastics for new materials production, *Nat. Rev. Chem.*, 2017, **1**(6), 0046.
- 5 J. Savoldelli, D. Tombac and H. Savoldelli, Breaking down polystyrene through the application of a two-step thermal degradation and bacterial method to produce usable byproducts, *Waste Manage.*, 2017, **60**, 123–126.
- 6 C. Jehanno, J. W. Alty, M. Roosen, S. De Meester, A. P. Dove, E. Y. X. Chen, F. A. Leibfarth and H. Sardon, Critical advances and future opportunities in upcycling commodity polymers, *Nature*, 2022, **603**(7903), 803–814.
- 7 X. Zhao, B. Boruah, K. F. Chin, M. Đokić, J. M. Modak and H. S. Soo, Upcycling to Sustainably Reuse Plastics, *Adv. Mater.*, 2021, 2100843.
- 8 C. W. S. Yeung, M. H. Periyah, J. Y. Q. Teo, E. T. L. Goh, P. L. Chee, W. W. Loh, X. J. Loh, R. Lakshminarayanan and J. Y. C. Lim, Transforming Polyethylene into Water-Soluble Antifungal Polymers, *Macromolecules*, 2023, **56**(3), 815–823.
- 9 J. Y. Q. Teo, A. Ong, T. T. Y. Tan, X. Li, X. J. Loh and J. Y. C. Lim, Materials from waste plastics for CO₂ capture and utilisation, *Green Chem.*, 2022, **24**, 6086–6099.
- 10 M. Y. Tan, L. Goh, D. Safanama, W. W. Loh, N. Ding, S. W. Chien, S. S. Goh, W. Thitsartarn, J. Y. C. Lim and D. W. H. Fam, Upcycling waste poly(ethylene terephthalate) into polymer electrolytes, *J. Mater. Chem. A*, 2022, **10**(46), 24468–24474.
- 11 Z. Xu, F. Pan, M. Sun, J. Xu, N. E. Munyaneza, Z. L. Croft, G. Cai and G. Liu, Cascade degradation and upcycling of polystyrene waste to high-value chemicals, *Proc. Natl. Acad. Sci. U.S.A.*, 2022, **119**(34), e2203346119.
- 12 A. Ong, J. Y. Q. Teo, Z. Feng, T. T. Y. Tan and J. Y. C. Lim, Organocatalytic Aerobic Oxidative Degradation of Polystyrene to Aromatic Acids, *ACS Sustainable Chem. Eng.*, 2023, **11**(34), 12514–12522.
- 13 *Market Volume of Benzoic Acid Worldwide From 2015 to 2020, With a Forecast for 2021 to 2026*, <https://www.statista.com/statistics/1245227/benzoic-acid-market-volume-worldwide/>, accessed 02 Feb 2023.
- 14 A. Pifer and A. Sen, Chemical Recycling of Plastics to Useful Organic Compounds by Oxidative Degradation, *Angew. Chem., Int. Ed.*, 1998, **37**(23), 3306–3308.
- 15 C. Rabot, Y. Chen, S.-Y. Lin, B. Miller, Y.-M. Chiang, C. E. Oakley, B. R. Oakley, C. C. C. Wang and T. J. Williams, Polystyrene Upcycling into Fungal Natural Products and a Biocontrol Agent, *J. Am. Chem. Soc.*, 2023, **145**(9), 5222–5230.
- 16 K. P. Sullivan, A. Z. Werner, K. J. Ramirez, L. D. Ellis, J. R. Bussard, B. A. Black, D. G. Brandner, F. Bratti, B. L. Buss, X. Dong, S. J. Haugen, M. A. Ingraham, M. O. Konev, W. E. Michener, J. Miscall, I. Pardo, S. P. Woodworth, A. M. Guss, Y. Román-Leshkov, S. S. Stahl and G. T. Beckham, Mixed plastics waste valorization through tandem chemical oxidation and biological funneling, *Science*, 2022, **378**(6616), 207–211.
- 17 Y. Zhang, M.-Y. Qi, Z.-R. Tang and Y.-J. Xu, Photoredox-Catalyzed Plastic Waste Conversion: Nonselective Degradation versus Selective Synthesis, *ACS Catal.*, 2023, **13**(6), 3575–3590.
- 18 S. Oh and E. E. Stache, Chemical Upcycling of Commercial Polystyrene via Catalyst-Controlled Photooxidation, *J. Am. Chem. Soc.*, 2022, **144**(13), 5745–5749.
- 19 Z. Huang, M. Shanmugam, Z. Liu, A. Brookfield, E. L. Bennett, R. Guan, D. E. Vega Herrera, J. A. Lopez-Sanchez, A. G. Slater, E. J. L. McInnes, X. Qi and J. Xiao, Chemical Recycling of Polystyrene to Valuable Chemicals via Selective Acid-Catalyzed Aerobic Oxidation under Visible Light, *J. Am. Chem. Soc.*, 2022, **144**(14), 6532–6542.
- 20 Y. Qin, T. Zhang, H. Y. V. Ching, G. S. Raman and S. Das, Integrated strategy for the synthesis of aromatic building blocks via upcycling of real-life plastic wastes, *Chem*, 2022, **8**(9), 2472–2484.
- 21 R. Cao, M.-Q. Zhang, C. Hu, D. Xiao, M. Wang and D. Ma, Catalytic oxidation of polystyrene to aromatic oxygenates over a graphitic carbon nitride catalyst, *Nat. Commun.*, 2022, **13**(1), 4809.
- 22 N. A. Romero and D. A. Nicewicz, Organic Photoredox Catalysis, *Chem. Rev.*, 2016, **116**(17), 10075–10166.
- 23 A. Tlili and S. Lakhdar, Acridinium Salts and Cyanoarenes as Powerful Photocatalysts: Opportunities in Organic Synthesis, *Angew. Chem., Int. Ed.*, 2021, **60**(36), 19526–19549.
- 24 B. Zilate, C. Fischer and C. Sparr, Design and application of aminoacridinium organophotoredox catalysts, *Chem. Commun.*, 2020, **56**(12), 1767–1775.



- 25 A. Soyemi and T. Szilvási, Trends in computational molecular catalyst design, *Dalton Trans.*, 2021, **50**(30), 10325–10339.
- 26 K. Ohkubo, K. Mizushima and S. Fukuzumi, Oxygenation and chlorination of aromatic hydrocarbons with hydrochloric acid photosensitized by 9-mesityl-10-methylacridinium under visible light irradiation, *Res. Chem. Intermed.*, 2013, **39**(1), 205–220.
- 27 A. A. Isse, C. Y. Lin, M. L. Coote and A. Gennaro, Estimation of Standard Reduction Potentials of Halogen Atoms and Alkyl Halides, *J. Phys. Chem. B*, 2011, **115**(4), 678–684.
- 28 S. Oh and E. E. Stache, Mechanistic Insights Enable Divergent Product Selectivity in Catalyst-Controlled Photooxidative Degradation of Polystyrene, *ACS Catal.*, 2023, 10968–10975.
- 29 P. Jia, Q. Li, W. C. Poh, H. Jiang, H. Liu, H. Deng and J. Wu, Light-Promoted Bromine-Radical-Mediated Selective Alkylation and Amination of Unactivated C(sp³)-H Bonds, *Chem*, 2020, **6**(7), 1766–1776.
- 30 S. Fukuzumi and K. Ohkubo, Organic synthetic transformations using organic dyes as photoredox catalysts, *Org. Biomol. Chem.*, 2014, **12**(32), 6059–6071.
- 31 C. Qin, T. Shen, C. Tang and N. Jiao, FeCl₂-Promoted Cleavage of the Unactivated C–C Bond of Alkylarenes and Polystyrene: Direct Synthesis of Arylamines, *Angew. Chem., Int. Ed.*, 2012, **51**(28), 6971–6975.
- 32 G. G. Gerosa, M. O. Marcarino, R. A. Spanevello, A. G. Suárez and A. M. Sarotti, Re-Engineering Organocatalysts for Asymmetric Friedel–Crafts Alkylation of Indoles through Computational Studies, *J. Org. Chem.*, 2020, **85**(15), 9969–9978.
- 33 K. N. Houk and P. H.-Y. Cheong, Computational prediction of small-molecule catalysts, *Nature*, 2008, **455**(7211), 309–313.
- 34 Y. Zou, J. J. Wong and K. N. Houk, Computational Exploration of a Redox-Neutral Organocatalytic Mitsunobu Reaction, *J. Am. Chem. Soc.*, 2020, **142**(38), 16403–16408.
- 35 N. Fey, Lost in chemical space? Maps to support organometallic catalysis, *Chem. Cent. J.*, 2015, **9**(1), 38.
- 36 C. Robertson and S. Habershon, Fast screening of homogeneous catalysis mechanisms using graph-driven searches and approximate quantum chemistry, *Catal. Sci. Technol.*, 2019, **9**(22), 6357–6369.
- 37 K. J. Kron, A. Rodriguez-Katakura, R. Elhessen and S. Mallikarjun Sharada, Photoredox Chemistry with Organic Catalysts: Role of Computational Methods, *ACS Omega*, 2021, **6**(49), 33253–33264.
- 38 S. Grimme, *Calculation of the Electronic Spectra of Large Molecules*, ed. K. B. Lipkowitz, R. Larter and T. R. Cundari, 2004.
- 39 C. Hansch, A. Leo and R. W. Taft, A survey of Hammett substituent constants and resonance and field parameters, *Chem. Rev.*, 1991, **91**(2), 165–195.
- 40 G. Jones, D. Yan, S. R. Greenfield, D. J. Gosztola and M. R. Wasielewski, Anilide Linker Group as a Participant in Intramolecular Electron Transfer, *J. Phys. Chem. A*, 1997, **101**, 4939–4942.
- 41 S. A. Jonker, F. Ariese and J. W. Verhoeven, Cation complexation with functionalized 9-arylacridinium ions: possible applications in the development of cation-selective optical probes, *Recl. Trav. Chim. Pays-Bas*, 1989, **108**(3), 109–115.
- 42 Z. Peng, R. Chen and H. Li, Heterogeneous Photocatalytic Oxidative Cleavage of Polystyrene to Aromatics at Room Temperature, *ACS Sustainable Chem. Eng.*, 2023, **11**(29), 10688–10697.
- 43 T. Li, A. Vijeta, C. Casadevall, A. S. Gentleman, T. Euser and E. Reisner, Bridging Plastic Recycling and Organic Catalysis: Photocatalytic Deconstruction of Polystyrene via a C–H Oxidation Pathway, *ACS Catal.*, 2022, **12**(14), 8155–8163.
- 44 M. Wen, X. Wang, T. Wang, Y. Sun, M. Fan, M. Li, J. Zhu, D. Zhang, X. Cui and Y. Shan, Acridinium Benzoates for Ratiometric Fluorescence Imaging, *Chem.–Eur. J.*, 2020, **26**(15), 3247–3251.
- 45 A. Scorilas, K. Agiamarnioti and K. Papadopoulos, Novel biotinylated acridinium derivatives: new reagents for fluorescence immunoassays and proteomics, *Clin. Chim. Acta*, 2005, **357**(2), 159–167.
- 46 A. Natrajan, D. Sharpe, J. Costello and Q. Jiang, Enhanced immunoassay sensitivity using chemiluminescent acridinium esters with increased light output, *Anal. Biochem.*, 2010, **406**(2), 204–213.

